ACI STRUCTURAL JOURNAL TECHNICAL PAPER

Title no. 87-S27

Thermal Gradient Effects in Reinforced Concrete Frame Structures

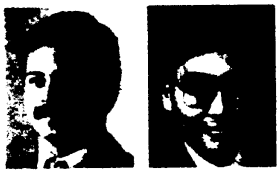

by Frank J. Vecchio and James A. Sato

Three large-scale reinforced concrete portal frame models were subjected to combinations of thermal and mechanical loads. Test conditions included unrestrained thermal deformation, restrained deformation under shock thermal loads, and loading to ultimate capacity. Aspects of response were monitored in terms of resulting restraint forces, deflections, strains, cracking, and leakage. Test results indicated that thermal loads can result in significant stressing of a structure and can lead to concentrated damage in local regions. A proposed theoretical analysis procedure was found to give reasonably accurate predictions of response.

Keywords: creep properties; deformation; **frames; reinforced concrete;** stresses; temperature; tests; **thermal gradient.**

Various analytical procedures[1-5] have been proposed for the analysis of thermal stresses in reinforced concrete frame structures. In general, these procedures attempt to account for reduced member stiffnesses when determining the moment distributions that arise from the restrained deformations of frames under thermal load. However, the proposed methods tend to be complicated or rely heavily on simplifying assumptions. Many do not adequately account for such factors as concrete tensile strength, tension-stiffening effects after cracking, simultaneously acting mechanical loads, force redistribution, nonlinear thermal gradients, or nonuniformly cracked members. Others resort to overly simplistic single-section analyses, ignoring overall structural response. Not surprisingly, the methods yield radically different results.[6] Unfortunately, little experimental data has been available to corroborate these proposed analysis procedures.

An alternative nonlinear approach[7] was recently suggested for the analysis of reinforced concrete frames subjected to thermal loads. It is distinct from previously proposed methods in that it incorporates sectional-response calculations into the overall frame analysis, taking into account nonlinear material behavior and time- and temperature-dependent effects.

An extensive test program was undertaken to provide the basic data required to calibrate and validate the theoretical formulation. The experimental program was also expected to address specific questions regarding the performance of concrete structures under high thermal gradient loads and to provide some insight into behavior. This paper summarizes the details and findings of the test program. Reference 8 gives a more detailed description and complete test results.

RESEARCH SIGNIFICANCE

The test findings described in this paper represent a large database useful for investigating the accuracy of current analytical procedures. As well, they serve to emphasize the behavioral concepts important to understanding and correctly modeling the response of reinforced concrete structures to thermal loads.

TEST PROGRAM

The experimental program consisted of three large-scale reinforced concrete frame models subjected to a total of 61 tests. The tests covered a diverse range of thermal and mechanical loading conditions.

Fig. 1 shows the test model. The configuration of the test model was essentially that of a simple portal frame consisting of two columns, each measuring 300 x 800 x 2350 mm (12 x 32 x 92 in.), and one beam measuring 300 x 800 x 2700 mm (12 x 32 x 106 in.) [see Fig. 1(b)]. The model sat in an inverted position on a reaction frame, with the ends of the columns connected by two 25 mm (1 in.) diameter tie-rods [see Fig. 1(a)]. Two reinforced concrete side panels spanned the interior of the frame to form a tanklike structure. Flexible silicone waterstops were used to bridge between the panels and the frame, which allowed the panels to be structurally independent and thus did not affect the frame's stiff-

ACI Structural Journal, V. 87, No. 3, May-June 1990.
Received Oct. 18, 1988 and reviewed under Institute publication policies.

ACI member Frank J. Vecchio is an associate professor of civil engineering at the University of Toronto. His research interests relate primarily to constitutive modeling, nonlinear analysis, and computer-aided design of reinforced concrete. Dr. Vecchio is a member of ACI Committee 435, Deflections of Concrete Building Structures, and of Canadian Standards Association CSA N287.3, Technical Committee on Concrete Containment Structures for Nuclear Power Plants.

ACI member James A. Sato is a research engineer at Ontario Hydro. A graduate of the University of Toronto, his research at Ontario Hydro is related to the design and development of reinforced concrete nuclear containment structures and the evaluation and development of polymer concretes.

ness or response. Water was placed in the tank to a depth of 1500 mm (60 in.), and a 120 kW immersion heater was used to apply thermal loads to the structure. The sides of the model were insulated to insure unidirectional heat flow from the inside to the outside surfaces. Mechanical loads were applied simultaneously by pretensioning the tie-rods, or by external forces applied through a 1000 kN (220 kip) servo-controlled actuator. The test models were instrumented extensively with load cells, thermocouples, strain gages, and displacement transducers to monitor response.

The amount of longitudinal reinforcement provided in the models' beams and columns was the primary variable in specimen construction. In Model PF1, the longitudinal reinforcement in both columns and in the beam was identical. In Model PF2, one column was more lightly reinforced than the remainder of the frame, whereas in Model PF3 the beam was more lightly reinforced than the columns. In all cases, the longitudinal reinforcement was symmetrically placed within the cross section, and adequate shear reinforcement was provided. Fig. 1(c) gives section details, and Table 1 provides reinforcement details.

The material properties of the concrete and reinforcement in each of the models are given in Table 2. The concrete cracking strengths shown were determined from split-cylinder tests, and the coefficients of thermal expansion for the concrete were calculated from results of tests on wet prisms. The thermal diffusivity of the concrete was measured for Model PF1 only; similar values were assumed for the other two models. The stress-strain response of the reinforcement was characterized by a long, flat yield plateau.

Each of the models was subjected to a multiphase test program involving three distinct types of thermal/mechanical load conditions (see Fig. 2 and Table 3). The test program was conducted such that each successive test represented a more damaging condition than the previous one. (Note that the alphabetical labeling of tests represents a chronological order, except that PF2-V precedes PF2-U.)

The Type I tests were conducted with the test models in an unrestrained mode with the tie-rods disengaged [see Fig. 2(a)]. The applied thermal loads involved up to three cycles of heating and cooling, with the load consisting of a 80 C (144 F) increase in internal temperature applied at a rate of 40 C/hr (72 F/hr). No mechanical load was applied. Conditions at each half-cycle

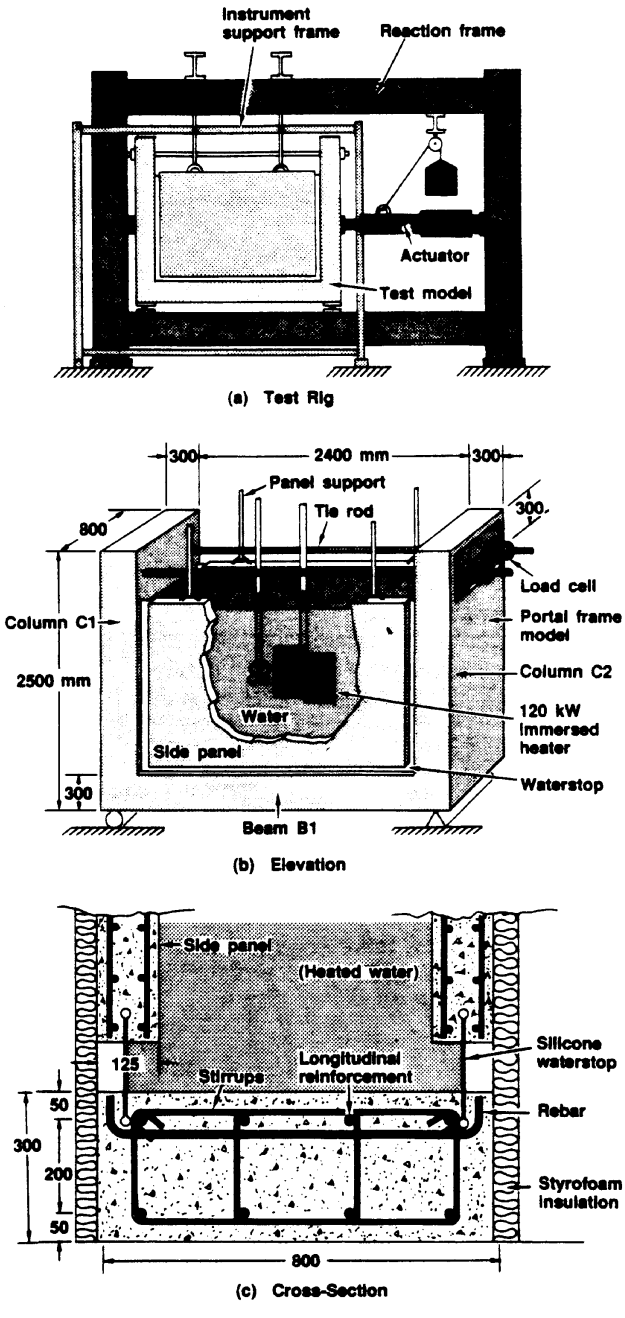

Fig. 1 — Test model details

(i.e., at 15 and 95 C) were maintained for 24 hr, so that both transient and final steady-state conditions could be monitored. Type I tests were conducted at the beginning of the overall test program (with the test models essentially uncracked) and again at the conclusion of the Type II tests (with the models extensively cracked).

In the Type II tests, the tie-rods were engaged to render the structure one-degree statically indeterminate [see Fig. 2(b)]. Thermal loads applied to the model resulted in the column ends tending to deflect outward. However, with the columns restrained from outward deflection by the tie-rods, restraint forces were induced in the tie-rods and hence in the frame. The Type II test program was subdivided into three series of tests, in which each series differed in the amount of preload placed in the tie-rods (before the application of thermal loads). In

Table 1 — Specimen details

			PF1	PF2	PF3
BEAM B1	b	(mm)	800	800	800
	h	(mm)	300	300	300
	A_s'	–	4#20M	3#20M/2#25M	3#20M
	d'	(mm)	55	50	50
	A_s	–	4#20M	3#20M/2#25M	3#20M
	d	(mm)	245	250	250
	A_v	–	#10M	#10M	#10M
	s	(mm)	150	150	150
COLUMN C1	b	(mm)	800	800	800
	h	(mm)	300	300	300
	A_s'	–	4#20M	3#20M/2#25M	3#20M/2#25M
	d'	(mm)	55	50	50
	A_s	–	4#20M	3#20M/2#25M	3#20M/2#25M
	d	(mm)	245	250	250
	A_v	–	#10M	#10M	#10M
	s	(mm)	150	150	150
COLUMN C2	b	(mm)	800	800	800
	h	(mm)	300	300	300
	A_s'	–	4#20M	3#20M	3#20M/2#25M
	d'	(mm)	55	50	50
	A_s	–	4#20M	3#20M	3#20M/2#25M
	d	(mm)	245	250	250
	A_v	–	#10M	#10M	#10M
	s	(mm)	150	150	150

Note: Area of #10M is 100 mm^2; #20M is 300 mm^2; #25M is 500 mm^2.

Table 2 — Material properties

			PF1	PF2	PF3
CONCRETE	f'_c	(MPa)	42.4	48.4	30.1
	f_{cr}	(MPa)	3.12	3.80	3.10
	E_c	(MPa)	28,980	33,500	30,000
	α_c	(/°C)	9.86×10^{-6}	11.9×10^{-6}	12.1×10^{-6}
REINFORCEMENT	f_y	(MPa)	448	448/452	450/445
	f_u	(MPa)	710	710/720	710/720
	E_s	(MPa)	217,000	200,000	200,000
	α_s	(/°C)	12.4×10^{-6}	12×10^{-6}	12×10^{-6}

Note:

1. For Models PF2 and PF3, f_y and f_u are given for 20M and 25M bars.
2. Thermal diffusivity for PF1 was measured at 0.774 mm^2/s.

the Type II Series I tests, a low level of preload was imparted to the tie-rods (see Table 3). In the Series II and III tests, moderate and high preloads, respectively, were applied to the tie-rods. For each series of tests,

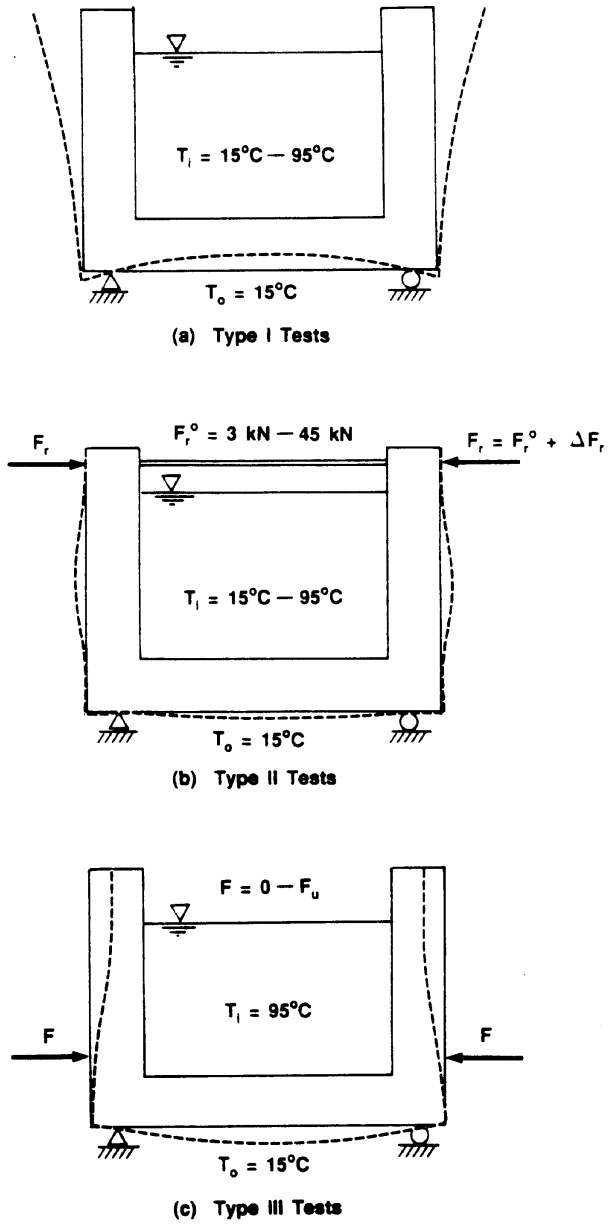

Fig. 2 — Loading conditions

shock thermal loads were applied ranging from 10 to 80 C (18 to 144 F). Thermal loads were applied at a rate of approximately 40 C/hr (72 F/hr) up to the test temperature; this temperature was then maintained for a 1 to 7-day duration. Instrument readings were taken at frequent intervals. Crack patterns were mapped and measured shortly after the peak thermal loads had been reached and again prior to the conclusion of the test.

In the Type III tests, the models were in the unrestrained configuration with the tie-rods disengaged [see Fig. 2(c)]. A large and constant thermal gradient was imposed on the structure throughout the test [*Ti* = 95 C (203 F)]. A simultaneously acting mechanical load was applied laterally to the columns at a location 680 mm (27 in.) above the centerline of the beam. The load was monotonically increased from zero, while the thermal gradient was held constant, until the ultimate capacity of the structure was attained.

TEST OBSERVATIONS

Type I tests

Condensed results of the Type I tests are summarized in Table 4. Typical response histories are shown in Fig. 3 for an uncracked specimen (Test PF3-B) and for an extensively cracked specimen (Test PF3-T).

During Type I testing, transient thermal gradients were created within the structural members. These gradients developed in a manner consistent with the computed response based on a standard unidirectional heat flow analysis. Thus, the gradients were exceedingly nonlinear shortly after loading (see Fig. 4). Steady-state conditions, characterized by a fairly linear gradient through the depth of the section, were achieved approximately 18 hr after the thermal loads were applied. At steady-state, the exterior surface temperature was significantly higher than the surrounding air temperature, reflecting a pronounced "skin effect." On the inside surface, where the contact medium was water, the surface temperature was essentially the same as the water temperature. The thermal gradients observed during the Type I tests on Model PF3 are shown in Fig. 3(a), which shows the two loading conditions to be virtually identical. Note that the drop-off in gradient shortly after peak is due to warming of the outside surface.

The imposed thermal loads resulted in an upward deflection of the beam relative to its ends, and outward deflections of the columns relative to their bases. These deflections occurred quickly following load application, with maximum deflections essentially attained within 2 hr. The total relative deflection of the columns, at tie-rod level, a distance of 2200 mm (86 in.) from the base, is shown in Fig. 3(b) for the Type I tests conducted on Model PF3. The deflections observed did not appear to be influenced to a significant extent by preexisting cracks, as little difference is seen between Test PF3-T (cracked) and Test PF3-B (uncracked) responses. Also note that the thermal loads resulted in a permanent residual deflection accumulating through each loading cycle, with the uncracked specimens exhibiting greater residual deflections than did the precracked specimens.

Primary thermal stresses were induced in the test models under Type I loading conditions. These arose primarily from nonlinearity in the thermal gradients shortly after loading but also from differences in coefficients of thermal expansion between concrete and reinforcement. A measure of these stresses was obtained from embedded strain gages, which were corrected for thermal strains. The concrete stresses computed were greatest ½ to 1 hr after peak thermal loading was achieved, with compressive stresses occurring near the inside and outside surfaces and tensile stresses in the middepth regions (see Fig. 4). As the thermal gradients approached linear steady-state conditions, the stresses in the concrete diminished. Compressive stresses were also found in the top and bottom reinforcement, determined from strain gages placed on the reinforcing bars. In the top reinforcement, located near the heated surface, these stresses tended to peak shortly after the ap-

Table 3 — Test parameters

MODEL	TEST MODE	MECHANICAL PRELOAD F_r° (kN)	THERMAL LOAD ΔT_i (°C)	DURATION (hr)
PF1-B	Type I	-	70	2 @ 48
PF1-C *	Type II	3.2	80	144
PF1-D	Type II	3.2	10	24
PF1-E	Type II	3.1	21	24
PF1-F	Type II	3.1	31	24
PF1-G	Type II	3.0	41	24
PF1-H	Type II	3.0	51	24
PF1-I	Type II	3.0	60	24
PF1-J	Type II	3.1	67	24
PF1-K	Type II	3.1	80	24
PF1-L	Type II	22.9	20	24
PF1-M	Type II	22.9	40	24
PF1-N	Type II	22.9	60	24
PF1-O	Type II	23.0	80	24
PF1-P	Type II	38.5	21	24
PF1-Q	Type II	38.2	41	24
PF1-R	Type II	38.4	60	24
PF1-S	Type II	39.1	78	24
PF1-T	Type I	-	70	48
PF1-U	Type III	-	80	4
PF2-A	Type I	-	80	3 @ 48
PF2-B	Type II	3.7	11	24
PF2-C	Type II	3.6	16	24
PF2-D	Type II	3.8	20	144
PF2-E	Type II	3.8	26	24
PF2-F	Type II	3.7	30	24
PF2-G	Type II	3.9	37	24
PF2-H	Type II	3.6	42	168
PF2-I	Type II	3.6	51	24
PF2-J	Type II	3.6	60	168
PF2-K	Type II	3.5	72	24
PF2-L	Type II	3.6	81	144
PF2-M	Type II	29.6	21	24
PF2-N	Type II	29.5	41	24
PF2-O	Type II	29.4	60	96
PF2-P	Type II	29.5	78	24
PF2-Q	Type II	44.1	22	24
PF2-R	Type II	44.4	42	24
PF2-S	Type II	44.3	60	12
PF2-T	Type II	44.2	78	24
PF2-V	Type I	-	65	48
PF2-U	Type III	-	80	4
PF3-B	Type I	-	78	3 @ 48
PF3-C	Type II	4.0	11	24
PF3-D	Type II	4.2	21	144
PF3-E	Type II	4.1	26	24
PF3-F	Type II	3.9	31	24
PF3-G	Type II	4.0	41	144
PF3-H	Type II	4.3	52	24
PF3-I	Type II	4.0	62	72
PF3-J	Type II	3.9	71	24
PF3-K	Type II	4.0	80	168
PF3-L	Type II	21.4	22	24
PF3-M	Type II	21.4	41	24
PF3-N	Type II	21.5	61	168
PF3-O	Type II	20.9	80	24
PF3-P	Type II	33.4	22	24
PF3-Q	Type II	33.2	41	24
PF3-R	Type II	33.2	60	168
PF3-S	Type II	32.6	80	24
PF3-T	Type I	-	80	3 @ 48

* Gradual heating condition.

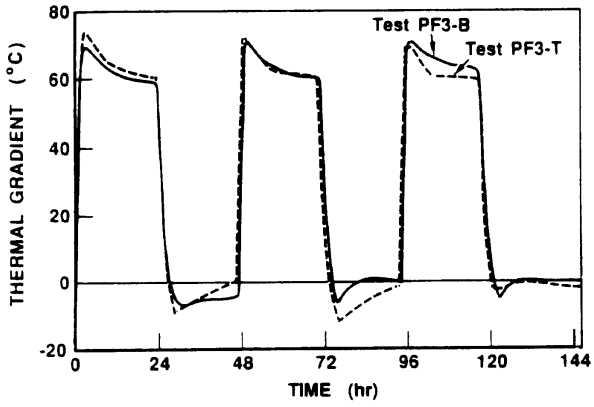

(a) Thermal Load Conditions

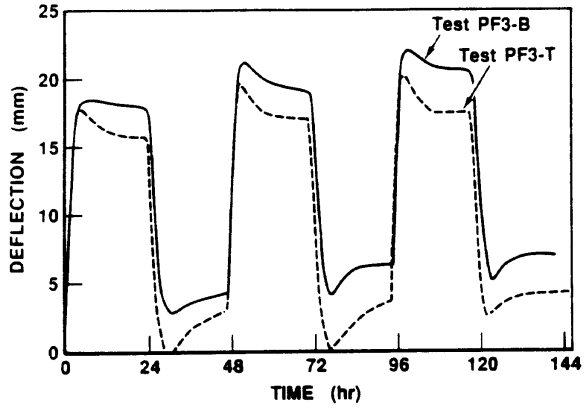

(b) Column Deflection

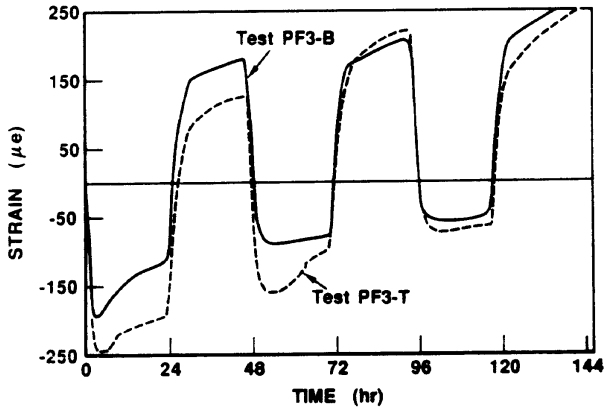

(c) Strain in Beam Top Rebar

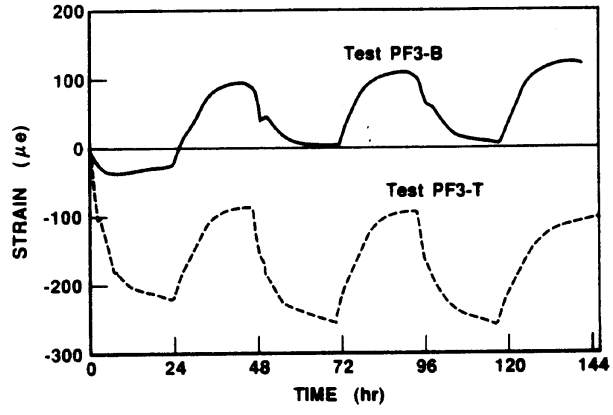

(d) Strain in Beam Bottom Rebar

Fig. 3 — Typical response observed in Type I test

plication of the load. The bottom reinforcement, located near the cooler face, showed a more gradual increase in stress and attained generally lower values [see Fig. 3 (c)].

No new visible cracks formed as a result of the Type I test conditions. However, the strains measured by embedded gages at middepths of the sections would indicate that internal cracks developed (see Fig. 4). Also, no leakage of water was noted during the Type I tests in either the uncracked or precracked specimens.

Type II tests

Representative results from the Type II tests are summarized in Tables 5 and 6. Table 5 reports data recorded shortly after the peak restraint forces had been attained in each test. In Table 6, the data given correspond to conditions just prior to the removal of thermal load, from 1 to 7 days after application. In Fig. 5, the response histories from a set of tests are given to illustrate typical behavior. The four tests summarized were all performed on the same specimen (Model PF3), with the same preload in the tie-rods (4.0 kN), but with the thermal load ranging from 20 to 80 C (36 to 144 F).

The thermal gradients reported in Tables 5 and 6 represent the difference between the average inside-surface and outside-surface temperatures of the test models. The gradients achieved during a particular test were greatest shortly after the maximum inside (water) temperature had been attained, typically 1 to 2 hr after the commencement of testing [see Fig. 5(a)]. However, it should be noted that the gradient at this time was highly nonlinear through the depth of the structure. Linear, steady-state conditions were achieved approximately 18 hr after load application, when the outside-surface temperature stabilized.

In each of the three models tested, as progressively higher thermal and mechanical loads were imposed, a progression of cracking was observed along the underside of the beam and in the lower exterior surfaces of the columns (see Fig. 6). In a typical test, any propagation of crack lengths or widening of crack widths would occur shortly after application of the thermal load. Crack widths and lengths would then remain essentially constant over the duration of the test. Upon unloading, the cracks would recover somewhat, but the residual width of the cracks would increase after each test.

The restraint forces induced in the models generally peaked within 2 hr after the peak thermal loads had been attained. The forces would then decrease gradually over the next 24 hr but in an amount greater than any decrease in the acting thermal gradient. Over the next 6 days, the decrease would continue but at a gradually diminishing rate. At the end of 7 days, the restraint forces remained relatively constant. The level of restraint force induced depended on the level of thermal load applied, but in less than direct proportion [see Fig. 5(b)]. Test results showed a gradual and progressive softening in stiffness as the models sustained cracking and, in some instances, yielding (e.g., at

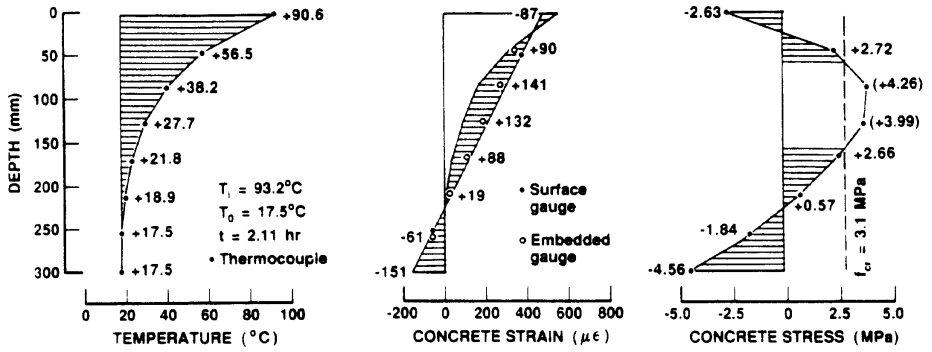

Fig. 4 — Transient conditions in an unrestrained section (Test PF3-B 2.1 hr after application of thermal load)

beam-column joint, Test PF2-S). The preload in the tie-rods was also seen to influence the thermal-restraint forces, since thermal loads coupled with these mechanical loads induced cracks that rendered the structures less stiff.

Specimens with larger amounts of reinforcement had higher restraint forces induced under a given thermal load due to increased member stiffness. For example, under similar thermal and mechanical load conditions, Model PF2 developed significantly higher thermal-induced forces than did Model PF3 (see Table 5). Finally, restraint forces were seen to be also influenced by the rate of thermal loading. The results of two series of tests performed on Model PF1, in which different heating rates were used, are shown in Fig. 7. The "shock-heating" envelope was obtained from tests performed under the Type II Series I program. The "gradual-heating" condition was obtained by applying a 5 C (9 F) increment every 8 hr (Test PF1-C). At the higher thermal-load levels, the shock loads resulted in significantly higher restraint forces being developed than did the gradual heating conditions. Note, however, that relatively lower forces were developed under shock-load conditions at the lower gradient levels. This anomaly is due to the Type II test program being preceded by Test PF1-C; thus, the model was precracked to some extent before the shock loads were applied.

Deformations in the models also followed consistent patterns. Column-end deflections were initially maintained at zero, through periodic adjustment of the tie-rods, to simulate the desired fixed-support condition. After the thermal load had been sustained for several hours, however, the column ends typically began to creep inward. The elongation of the bottom beam oc-

Table 4 — Results of Type I tests

TEST	F_r° (kN)	T_1 (°C)	T_2 (°C)	ΔT_l (°C)	t (hr)	T_1' (°C)	T_2' (°C)	ΔT_g (°C)	F_r' (kN)	δ_a (mm)	δ_b (mm)	δ_c (mm)	ϵ_{sbt} (με)	ϵ_{sbb} (με)	ϵ_{sct} (με)	ϵ_{scb} (με)
PF1-B	0.0	21.0	18.7	69.5	48.0	89.2	35.6	51.3	0.0	1.156	-1.023	12.446	N/A	N/A	N/A	N/A
					216.0	22.9	19.1	1.4	0.0	0.198	-0.137	2.208	N/A	N/A	N/A	N/A
PF1-T	0.0	15.5	19.5	70.0	24.0	84.8	28.6	60.2	0.0	0.912	-1.553	16.626	N/A	N/A	N/A	N/A
PF2-A	0.0	14.7	14.3	80.0	24.0	90.7	32.6	57.7	0.0	1.374	-1.624	18.862	-34	-2	-111	-76
					48.0	16.7	17.7	-1.4	0.0	0.266	-0.468	5.531	180	46	60	-1
					72.0	93.3	33.0	59.9	0.0	1.596	-1.805	20.302	-9	10	-93	-70
					96.0	15.6	17.2	-2.0	0.0	0.369	-0.547	6.569	235	65	87	11
					120.0	93.4	32.3	60.7	0.0	1.464	-1.802	21.181	18	14	-79	-60
					168.0	14.6	16.7	-2.6	0.0	0.348	-0.606	7.235	270	84	107	15
PF2-V	0.0	19.9	20.6	65.0	24.0	82.9	32.5	51.1	0.0	0.820	-1.192	13.209	-160	-84	-261	-85
PF3-B	0.0	16.4	16.1	78.0	24.0	91.8	31.9	59.6	0.0	1.222	-1.654	17.944	-118	-29	-13	-35
					48.0	12.9	16.8	-4.3	0.0	0.313	-0.347	4.358	178	86	135	26
					72.0	92.1	31.0	60.8	0.0	1.351	-1.718	19.059	-83	1	15	-29
					96.0	16.7	16.5	-0.2	0.0	0.468	-0.494	6.356	205	101	165	38
					120.0	92.3	29.0	63.0	0.0	1.471	-1.813	20.565	-57	3	34	-11
					144.0	13.8	14.1	-0.7	0.0	0.538	-0.521	7.004	245	120	196	55
PF3-T	0.0	13.6	14.5	80.0	24.0	92.5	32.6	61.0	0.0	N/A	-1.603	15.769	-196	-225	-56	-110
					48.0	15.2	15.9	0.2	0.0	N/A	-0.382	2.977	128	-92	38	-30
					72.0	92.7	32.9	60.7	0.0	N/A	-1.770	17.135	-102	-257	-131	-116
					96.0	14.7	17.8	-2.0	0.0	N/A	-0.473	3.599	219	-97	55	-44
					120.0	92.7	33.7	60.0	0.0	N/A	-1.818	17.566	-68	-261	-110	-126
					168.0	15.0	17.7	-1.5	0.0	N/A	-0.568	4.543	250	-103	88	-45

curred gradually with the rise in thermal load, stabilizing only after steady-state thermal conditions were attained. The magnitude of the elongation was essentially in linear proportion to the magnitude of the applied thermal gradient. The beam midspan deflections, conversely, were very sensitive to crack/yield conditions within the structure. The general trend was for a downward deflection to attain a peak value within approximately 2 hr of the peak thermal load and then remain essentially constant thereafter [see Fig. 5(c)].

Strains in the beam and column reinforcing bars were monitored at several locations. The beam reinforcing bar strains reported in Tables 5 and 6 are those measured at the midspan; the column reinforcing bar strains are those directly above the column-beam joint in Column C2. In all cases, the strains reported are increments in strain due to the applied thermal load. Thermal strains and initial strains due to the preloads in the tie-rods or the self-weight of the model have been factored out. The thermal loads generally caused compressive strains in the inside reinforcement and tensile strains in the outside reinforcement of both the beam and columns. In the compression reinforcement, the strains developed gradually over 6 to 12 hr after loading, eventually leveling off and not showing much decrease. The strains in the tensile reinforcement typically peaked within 2 to 3 hr of loading and then decreased significantly with time (up to 50 percent loss), stabiliz-

Table 5 — Results of Type II tests at time of peak restraint force

TEST	F_r° (kN)	T_1 (°C)	T_2 (°C)	ΔT_l (°C)	t (hr)	T_1' (°C)	T_2' (°C)	ΔT_g (°C)	F_r' (kN)	δ_a (mm)	δ_b (mm)	δ_c (mm)	ϵ_{sbt} ($\mu\epsilon$)	ϵ_{sbb} ($\mu\epsilon$)	ϵ_{sct} ($\mu\epsilon$)	ϵ_{scb} ($\mu\epsilon$)
PF1-D	3.17	17.7	15.2	10.4	1.92	27.6	15.4	9.7	7.10	0.067	0.095	-0.018	-20	80	10	90
PF1-E	3.05	14.9	14.8	21.2	2.26	35.4	14.8	20.5	10.66	0.181	0.188	-0.008	-50	180	-50	30
PF1-F	3.09	16.2	14.8	30.9	2.56	46.1	14.7	30.1	13.97	0.286	0.275	0.003	-100	230	-70	50
PF1-G	3.04	14.6	14.9	40.9	2.42	54.1	15.4	39.0	16.05	0.358	0.329	-0.027	-120	340	-40	90
PF1-H	3.03	14.9	15.1	50.6	2.43	64.1	15.2	49.2	17.94	0.420	0.390	-0.006	-140	430	-70	80
PF1-I	3.02	14.8	13.8	59.8	2.47	72.6	14.1	57.6	19.83	0.515	0.417	0.000	-150	480	-50	90
PF1-J	3.05	16.6	14.6	67.2	2.78	80.8	16.1	62.8	21.93	0.616	0.492	-0.002	-200	530	-110	100
PF1-K	3.06	13.1	13.5	79.4	3.21	89.9	16.1	74.4	25.64	0.766	0.588	0.008	-220	640	-170	90
PF1-L	22.91	15.7	17.2	19.8	1.32	35.0	17.9	18.7	26.56	0.133	0.064	-0.005	20	140	-20	160
PF1-M	22.85	16.3	15.1	40.3	1.67	55.4	14.7	39.5	30.10	0.304	0.139	0.001	-70	320	30	280
PF1-N	22.91	13.5	14.8	59.6	2.30	71.9	14.5	58.7	33.52	0.522	0.135	-0.002	-80	490	20	870
PF1-O	23.05	13.4	15.8	79.6	2.34	90.9	16.4	77.0	38.00	0.642	0.308	-0.001	-70	680	90	630
PF1-P	38.46	15.3	16.2	20.8	1.81	35.6	17.0	19.5	40.90	0.187	0.071	0.006	-60	130	-50	170
PF1-Q	38.19	13.6	16.1	40.8	1.45	53.2	15.9	39.8	44.64	0.317	0.119	-0.007	-90	210	50	340
PF1-R	38.36	14.0	15.3	60.4	1.73	72.6	15.8	58.0	45.90	0.462	0.206	-0.002	-110	360	30	N/A
PF1-S	39.11	17.0	16.7	77.6	2.05	92.5	17.9	74.2	50.06	0.639	0.296	0.018	-110	460	60	N/A
PF2-B	3.72	16.3	17.3	11.3	2.50	27.0	17.5	10.5	9.83	0.060	0.013	-0.004	-68	19	-62	23
PF2-C	3.60	16.3	15.6	15.9	2.60	31.3	15.6	15.1	13.76	0.106	0.029	0.004	-95	29	-76	36
PF2-D	3.76	15.9	15.2	19.5	2.26	34.3	16.1	17.5	15.76	0.081	0.018	0.011	-116	39	-89	38
PF2-E	3.83	17.4	15.8	26.0	1.91	41.8	16.3	23.9	20.06	0.102	0.023	0.001	-145	48	-117	64
PF2-F	3.70	18.4	16.3	30.0	1.30	46.1	16.6	27.4	19.40	0.084	0.014	0.001	-139	42	-107	99
PF2-G	3.89	16.4	15.7	36.7	1.96	50.4	16.3	33.4	21.75	0.159	-0.026	-0.001	-180	54	-108	633
PF2-H	3.59	13.0	13.6	42.3	2.34	52.8	15.0	38.4	22.84	0.232	0.069	0.003	-207	86	-128	682
PF2-I	3.55	13.3	13.6	50.9	2.10	61.1	14.8	46.6	25.46	0.268	0.089	0.003	-234	117	-128	779
PF2-J	3.59	14.4	14.8	60.0	2.34	70.8	15.7	55.5	26.73	0.411	0.145	0.004	-257	240	-136	883
PF2-K	3.54	15.4	13.6	72.2	2.36	82.7	15.0	65.8	29.64	0.477	0.185	-0.005	-296	260	-162	1016
PF2-L	3.64	13.1	12.5	80.7	2.69	88.7	14.1	74.1	30.63	0.589	0.118	0.002	-327	299	-164	1046
PF2-M	29.55	13.9	16.5	21.2	1.43	33.6	17.3	18.9	34.38	0.107	-0.058	0.002	-75	52	-15	215
PF2-N	29.53	15.6	13.6	40.8	1.38	53.2	14.0	37.2	39.70	0.217	-0.013	-0.001	-119	97	2	467
PF2-O	29.40	16.3	15.4	59.8	2.15	71.9	17.1	53.9	42.82	0.408	-0.116	-0.009	-206	184	-4	634
PF2-P	29.47	15.5	15.8	78.3	2.38	88.9	17.5	71.7	48.12	0.576	-0.037	0.002	-241	249	-17	975
PF2-Q	44.06	14.4	16.0	21.5	1.73	35.0	16.9	19.7	48.83	0.141	-0.034	0.006	-78	56	-6	248
PF2-R	44.43	16.7	19.2	41.9	1.85	55.5	20.3	37.7	53.68	0.285	-0.091	0.002	-141	118	18	624
PF2-S	44.29	18.7	19.1	59.8	1.96	74.6	20.8	54.2	54.68	0.412	-0.221	0.002	-181	158	128	8744
PF2-T	44.16	16.3	17.3	77.9	2.37	88.9	19.3	70.7	58.10	0.518	-0.339	0.007	-249	206	191	969
PF3-C	4.03	15.1	16.2	11.0	2.23	25.3	16.8	9.6	7.85	0.063	0.021	0.000	-71	19	-39	11
PF3-D	4.20	18.8	15.5	20.8	0.89	37.7	15.6	18.8	11.98	0.062	0.023	-0.003	-89	24	-36	22
PF3-E	4.06	16.8	15.1	25.8	1.52	40.7	15.8	23.3	13.15	0.133	0.128	0.000	-132	35	-60	25
PF3-F	3.85	15.8	16.6	31.0	2.17	44.9	17.4	28.3	14.64	0.155	0.270	0.009	-169	86	-79	31
PF3-G	4.00	16.2	15.9	40.9	2.34	54.7	16.6	37.7	15.78	0.196	0.432	0.001	-195	115	-94	32
PF3-H	4.34	14.5	14.0	52.0	2.61	63.5	14.5	48.6	18.11	0.233	0.677	0.003	-249	550	-123	44
PF3-I	3.96	14.7	14.4	61.9	2.86	73.0	16.0	56.7	19.49	0.211	0.748	0.002	-287	619	-143	50
PF3-J	3.86	13.9	14.5	70.9	2.61	80.3	15.8	65.2	20.49	0.180	0.741	0.001	-293	662	-149	55
PF3-K	3.98	14.4	14.7	80.4	3.34	90.3	17.9	72.6	21.41	0.281	0.811	0.013	-356	701	-180	57
PF3-L	21.4	13.2	10.9	22.3	1.65	33.7	11.2	20.3	25.07	0.080	0.192	0.006	-81	164	-41	24
PF3-M	21.4	14.4	13.5	40.5	1.44	51.5	14.1	36.6	28.62	0.174	0.302	0.000	-120	269	-50	38
PF3-N	21.5	13.1	13.0	60.5	2.17	69.7	14.4	55.1	31.81	0.304	0.517	-0.002	-216	428	-91	78
PF3-O	20.9	14.5	14.5	80.1	3.14	90.2	15.7	74.4	35.00	0.533	0.782	-0.004	-318	590	-147	123
PF3-P	33.4	13.4	13.0	22.3	1.72	34.0	14.1	19.6	36.19	0.102	0.164	0.012	-80	149	-34	23
PF3-Q	33.2	15.1	15.8	41.1	1.85	53.2	15.8	38.2	39.48	0.208	0.337	0.005	-141	302	-59	56
PF3-R	33.2	15.2	16.2	59.8	2.14	70.7	17.3	54.3	40.90	0.260	0.478	-0.003	-210	412	-83	75
PF3-S	32.6	15.9	16.0	79.2	2.40	89.7	17.3	72.5	43.41	0.382	0.617	-0.003	-263	526	-102	160

ing after 24 hr [see Fig. 5(d)]. At low load levels, abrupt changes occurred in the tensile reinforcement strain as thermal loads were increased and cracking was initiated [Fig. 5(d)]. However, in well-cracked sections, the strains were less dependent on mechanical load levels or on changes in crack conditions elsewhere in the structure. They were, however, still sensitive to the relative stiffness of the component members of the structure, as can be seen by comparing results for Tests PF2-L and PF3-K (see Table 6). Strains induced in the compression reinforcement were less sensitive to cracking and stiffness changes. These strains were almost linearly related to the level of thermal load applied.

No leakage of water through cracks was observed when the models were under load but with the reinforcement not yielded. At the conclusion of many tests, some minor leakage was observed as the thermal loads were removed and the compressive forces on the inside faces were relieved. At advanced stages of loading of PF2, where yielding of the reinforcement occurred at the base of the column, significant leakage through the cracks was observed.

Type III tests

In Type III testing, the models were under a constant thermal gradient of about 55 C (100 F). Lateral loads

Table 6 — Results of Type II tests at test conclusion

TEST	F_r° (kN)	T_1 (°C)	T_2 (°C)	ΔT_1 (°C)	t (hr)	T_1' (°C)	T_2' (°C)	ΔT_g (°C)	F_r (kN)	δ_a (mm)	δ_b (mm)	δ_c (mm)	ϵ_{sbt} ($\mu\epsilon$)	ϵ_{sbb} ($\mu\epsilon$)	ϵ_{sct} ($\mu\epsilon$)	ϵ_{scb} ($\mu\epsilon$)
PF1-D	3.17	17.7	15.2	10.4	24.0	25.0	15.7	6.8	5.30	0.161	0.122	-0.112	-100	-70	-100	10
PF1-E	3.05	14.9	14.8	21.2	24.0	35.8	17.9	17.8	7.93	0.380	0.201	-0.105	-180	100	-210	-100
PF1-F	3.09	16.2	14.8	30.9	24.0	46.5	22.3	22.9	9.00	0.500	0.287	-0.120	-150	100	-150	-120
PF1-G	3.04	14.6	14.9	40.9	24.0	54.6	25.2	29.7	10.92	0.726	0.326	-0.142	-160	150	-120	-40
PF1-H	3.03	14.9	15.1	50.6	24.0	65.0	23.6	41.7	14.15	0.854	0.437	-0.106	-220	220	-210	-120
PF1-I	3.02	14.8	13.8	59.8	24.0	73.7	23.4	49.4	15.21	1.038	0.491	-0.094	-230	260	-220	-100
PF1-J	3.05	16.6	14.6	67.2	24.0	78.3	26.3	50.0	15.97	1.123	0.548	-0.104	-240	290	-220	-120
PF1-K	3.06	13.1	13.5	79.4	24.0	91.1	29.6	62.0	18.84	1.396	0.650	-0.044	-320	350	-290	-170
PF1-L	22.91	15.7	17.2	19.8	24.0	35.5	20.7	16.4	23.04	0.333	0.075	-0.035	-10	100	-50	160
PF1-M	22.85	16.3	15.1	40.3	24.0	56.0	25.9	28.9	22.94	-0.630	0.087	-0.015	-160	140	-140	120
PF1-N	22.91	13.5	14.8	59.6	24.0	72.7	29.5	44.4	25.18	0.994	0.059	-0.036	-210	180	-170	470
PF1-O	23.05	13.4	15.8	79.6	24.0	92.4	31.5	63.4	27.78	1.399	0.404	-0.043	-310	370	-190	290
PF1-P	38.46	15.3	16.2	20.8	24.0	35.9	20.8	16.1	38.65	0.327	0.098	-0.015	-70	70	-80	90
PF1-Q	38.19	13.6	16.1	40.8	24.0	54.1	24.2	32.4	39.88	0.707	0.237	-0.026	-200	-30	-140	120
PF1-R	38.36	14.0	15.3	60.4	24.0	73.9	27.4	47.8	40.45	1.073	0.338	-0.013	-250	130	-90	N/A
PF1-S	39.11	17.0	16.7	77.6	24.0	93.9	34.0	59.5	45.88	1.299	0.238	-0.014	-260	220	-30	N/A
PF2-B	3.72	16.3	17.3	11.3	24.0	27.5	17.9	10.7	9.10	0.194	0.060	-0.020	-61	16	-65	25
PF2-C	3.60	16.3	15.6	15.9	24.0	31.6	18.5	12.5	10.23	0.219	0.074	-0.051	-89	11	-74	24
PF2-D	3.76	15.9	15.2	19.5	144.0	35.1	20.3	14.1	10.21	0.263	0.078	-0.050	-114	10	-86	14
PF2-E	3.83	17.4	15.8	26.0	24.0	42.8	21.5	19.6	12.46	0.384	0.112	-0.080	-134	29	-125	85
PF2-F	3.70	18.4	16.3	30.0	24.0	47.7	22.4	23.1	12.26	0.463	0.037	-0.109	-144	22	-141	570
PF2-G	3.89	16.4	15.7	36.7	24.0	52.2	24.0	27.5	12.24	0.581	0.209	-0.097	-177	61	-134	342
PF2-H	3.59	13.0	13.6	42.3	168.0	54.4	22.5	32.4	11.55	0.709	0.249	-0.112	-192	89	-145	325
PF2-I	3.55	13.3	13.6	50.9	24.0	63.4	26.1	37.5	14.08	0.792	0.220	-0.062	-232	144	-170	388
PF2-J	3.59	14.4	14.8	60.0	168.0	73.6	25.9	48.2	14.94	1.074	0.325	-0.126	-231	197	-176	478
PF2-K	3.54	15.4	13.6	72.2	24.0	86.0	28.4	55.8	19.16	1.235	0.301	-0.060	-303	192	-255	600
PF2-L	3.64	13.1	12.5	80.7	144.0	92.1	30.1	61.4	16.65	1.381	0.228	-0.026	-165	210	-220	509
PF2-M	29.55	13.9	16.5	21.2	24.0	34.9	22.2	15.4	29.80	0.341	0.006	-0.023	-82	15	-47	29
PF2-N	29.53	15.6	13.6	40.8	24.0	55.7	23.3	30.4	31.87	0.703	0.103	-0.048	-156	69	-79	145
PF2-O	29.40	16.3	15.4	59.8	96.0	75.4	30.8	43.7	32.19	1.042	0.003	-0.095	-182	116	-7	183
PF2-P	29.47	15.5	15.8	78.3	24.0	92.8	33.5	59.5	38.87	1.352	0.162	-0.024	-220	166	-168	532
PF2-Q	44.06	14.4	16.0	21.5	24.0	35.7	20.4	16.9	45.30	0.369	0.030	-0.032	-87	34	-48	105
PF2-R	44.43	16.7	19.2	41.9	24.0	57.8	26.7	33.7	47.51	0.748	0.082	-0.064	-158	127	-70	295
PF2-S	44.29	18.7	19.1	59.8	12.0	77.7	31.1	47.0	49.81	0.983	-0.135	-0.008	-222	109	4	10,070
PF2-T	44.16	16.3	17.3	77.9	24.0	93.1	35.8	58.3	47.46	1.299	-0.214	-0.038	-316	113	39	570
PF3-C	4.03	15.1	16.2	11.0	24.0	25.7	18.9	8.0	6.41	0.100	0.053	-0.019	-70	6	-40	1
PF3-D	4.20	18.8	15.5	20.8	144.0	39.7	18.3	18.0	7.95	0.303	0.318	-0.040	-121	8	-65	8
PF3-E	4.06	16.8	15.1	25.8	24.0	41.9	21.4	18.9	8.62	0.251	0.308	-0.049	-146	66	-83	-10
PF3-F	3.85	15.8	16.6	31.0	24.0	46.2	22.3	24.7	10.17	0.274	0.356	-0.044	-180	101	-99	2
PF3-G	4.00	16.2	15.9	40.9	144.0	56.1	24.3	31.4	8.56	0.376	0.604	-0.076	-188	436	-114	-6
PF3-H	4.34	14.5	14.0	52.0	24.0	65.3	22.3	42.7	11.94	0.404	0.695	-0.078	-275	346	-156	8
PF3-I	3.96	14.7	14.4	61.9	72.0	75.0	24.5	50.2	12.16	0.402	0.675	-0.068	-284	359	-171	12
PF3-J	3.86	13.9	14.5	70.9	24.0	83.3	27.6	56.4	13.90	0.474	0.690	-0.062	-207	376	-202	-2
PF3-K	3.98	14.4	14.7	80.4	168.0	93.1	30.9	62.4	11.79	0.512	0.923	-0.076	-292	343	-163	33
PF3-L	21.4	13.2	10.9	22.3	24.0	34.1	16.4	15.4	22.06	0.187	0.165	-0.013	-105	64	-68	9
PF3-M	21.4	14.4	13.5	40.5	24.0	54.1	22.2	31.0	24.18	0.376	0.321	-0.013	-195	124	-116	35
PF3-N	21.5	13.1	13.0	60.5	168.0	72.3	28.2	44.0	23.85	0.652	0.375	-0.040	-293	112	-142	20
PF3-O	20.9	14.5	14.5	80.1	24.0	92.8	30.4	62.3	30.16	0.879	0.751	-0.001	-382	325	-201	45
PF3-P	33.4	13.4	13.0	22.3	24.0	35.0	19.5	15.1	34.33	0.196	0.137	0.024	-109	55	-63	-9
PF3-Q	33.2	15.1	15.8	41.1	24.0	55.1	23.9	32.0	36.71	0.372	0.315	-0.013	-209	136	-113	16
PF3-R	33.2	15.2	16.2	59.8	168.0	73.8	29.6	45.2	35.92	0.538	0.362	-0.021	-297	144	-123	20
PF3-S	32.6	15.9	16.0	79.2	24.0	93.5	32.0	61.5	38.85	0.826	0.688	-0.014	-370	358	-190	49

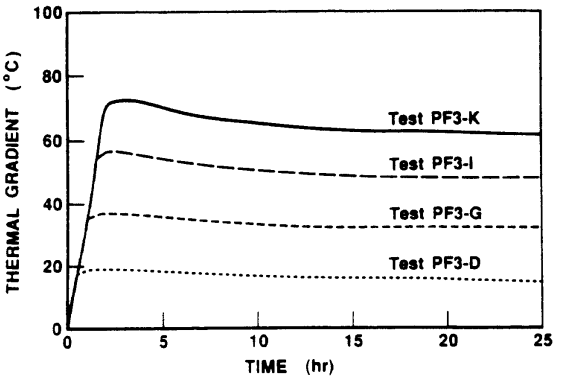

(a) Thermal Load Conditions

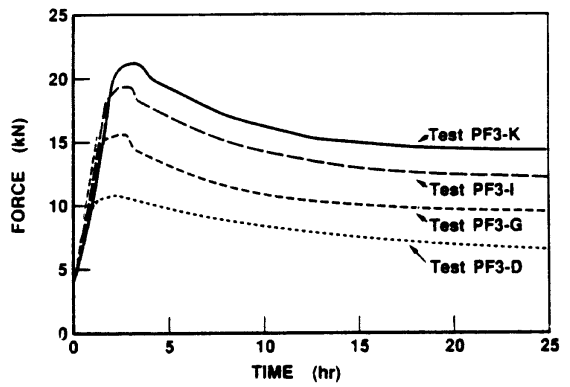

(b) Restraint Force

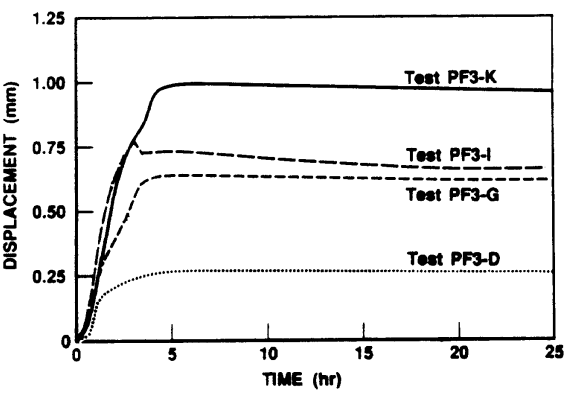

(c) Beam Deflection

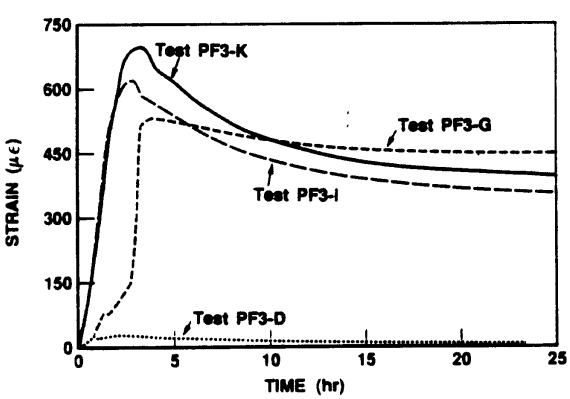

(d) Strain in Beam Bottom Rebar

Fig. 5 — Typical response observed in Type II test

applied to the columns were progressively increased until the ultimate capacities of the specimens were exceeded (see Fig. 8).

The deformation of the structure was linear with external load until yielding of the reinforcement occurred, either in the beam (Test PF1-U) or in the column (Test PF2-U). Thereafter, response was essentially plastic with a minimal increase in load capacity due to strain hardening. Both the preyield stiffness and the ultimate load capacity were approximately equal to predicted values using standard cracked-section anlayses.

The presence of a thermal gradient did not appear to affect the structural response in any way, other than possibly reducing by a minimal amount the yield strength of the reinforcement. However, the models were statically determinate in the Type III tests, with no possibility for redistribution of forces. It is likely that thermal gradients would have a more significant influence on the ultimate conditions of an indeterminate structure.

There was no leakages of water through the structural cracks as the mechanical load was applied. When the mechanical load was removed, but the thermal gradient was still present, some minor leakage occurred. The highest leakage rate observed was estimated to be approximately 0.015 ℓ/hr (6.6×10^{-6} gpm) through a single crack. After the model had cooled to room temperature, the leakage rate increased dramatically to as high as 0.10 ℓ/hr (0.44×10^{-3} gpm). Note, however, that the interior surfaces were essentially uncracked due to the nature of the loading conditions imposed. If the models were to experience loads resulting in reverse flexure, it is anticipated that the leakage would be significantly greater.

DISCUSSION OF TEST RESULTS

The most critical time in the response of the models to thermal loads was found to be shortly after the load was imposed. Primary stresses in the concrete, restraint forces in the members, strains in the tensile reinforcement, deflections of the structure, and crack widths all attained peak values within a short time (2 to 3 hr) after the thermal load had been applied, even though the thermal gradient through the depth of the structural members was still highly nonlinear. In the time required for steady-state conditions to be achieved (and hence, for the gradient to become linear), a significant degree of relaxation occurred. Thus, the definition of an effective thermal gradient should be primarily based on changes in near-surface temperatures, with not so much emphasis given to internal steady-state conditions.

The magnitude of restraint forces induced in the models under the various test conditions clearly indicated the importance of several factors commonly overlooked. First, there was a gradual transition from uncracked to cracked section response, arising from tension-stiffening effects in the concrete after cracking. To assume cracked-section stiffness in determining re-

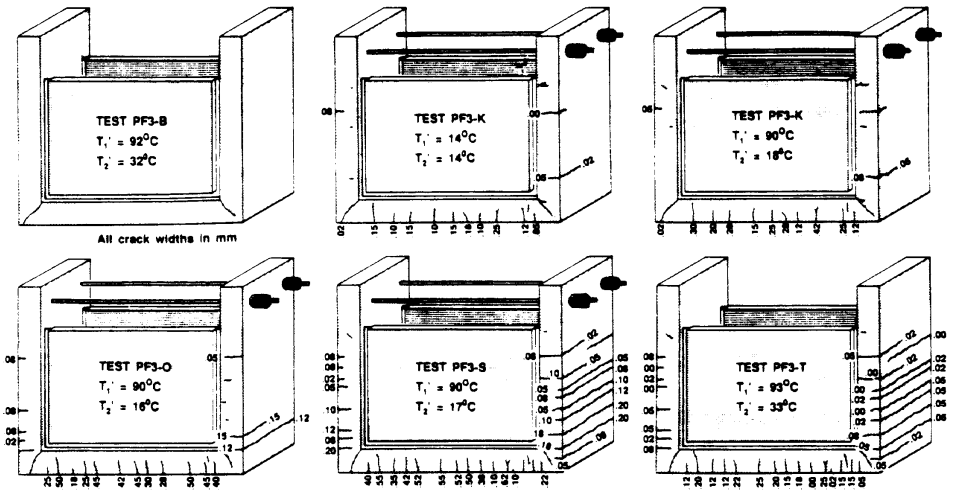

Fig. 6 — Progression of cracking observed in Model PF3

straint forces induced from thermal loads would result in a significant underestimation of these forces. Second, the forces developed at a particular location depended on overall structural behavior, that is, on the relative stiffness changes that occurred in all structural members due to progressive cracking and yielding. Analyzing a section's response in isolation by considering fixed-end conditions could result in either an over- or underestimation of force. Third, simultaneously acting mechanical loads were also significant in that they too impacted on the relative stiffness of components in the structure. The effects of thermal loads and mechanical loads are interdependent and cannot be analyzed separately. Finally, adding more reinforcement in a reinforced concrete structure serves to increase the thermal forces developed, rather than alleviate stresses as would be intended. To reinforce heavily some members can lead to overstressing in other regions of the structure. All these factors indicate that the restraint forces developed at a particular section or member are significantly influenced by conditions throughout the structure. A proper analysis must consider overall structural response to combined thermal/mechanical loads, giving adequate attention to tension-stiffening effects and force redistributions.

The high thermal and mechanical loads imposed in Tests PF2-S and PF2-T resulted in severe cracking and yielding in a localized area of the test specimen (at the base of Column C2). These results clearly showed that under certain conditions concentrated damage due to thermal deformation can occur in weaker regions of a structure. The damage can include excessively high straining or yielding of the reinforcement, large crack widths, and the formation of leakage paths. This damage will occur despite a minimal increase in restraint force accompanying the thermal loads. Hence, as when analyzing restraint forces, the deformations at a particular point in a structure can only be properly assessed by considering the overall structural response. An isolated section analysis assuming fixed-end conditions is inadequate, because under thermal loading, stiffer

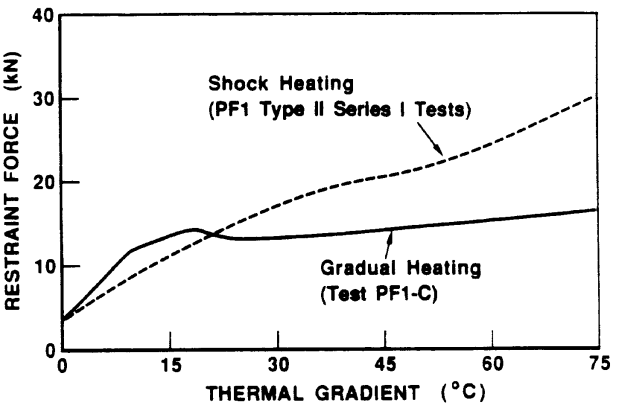

Fig. 7 — Influence of loading rate on Type II test response

Fig. 8 — Model PF2 prior to Type III testing

members may impose concentrated deformation on weaker members in an indeterminate structure.

A significant relaxation in restraint forces was observed over periods of time as short as 24 hr. Fig. 9 shows the force relaxations observed in the Type II tests, plotted against temperature. The restraint force

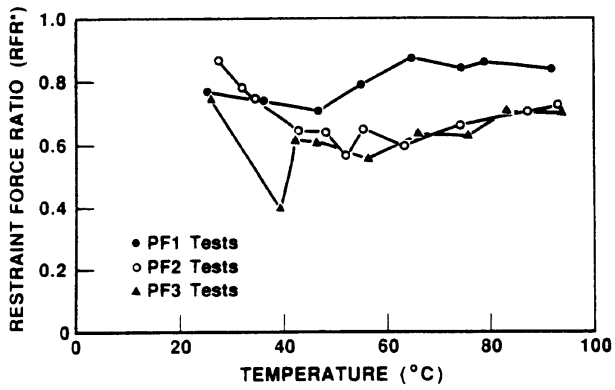

(a) Type II Series I Tests at 24 Hrs.

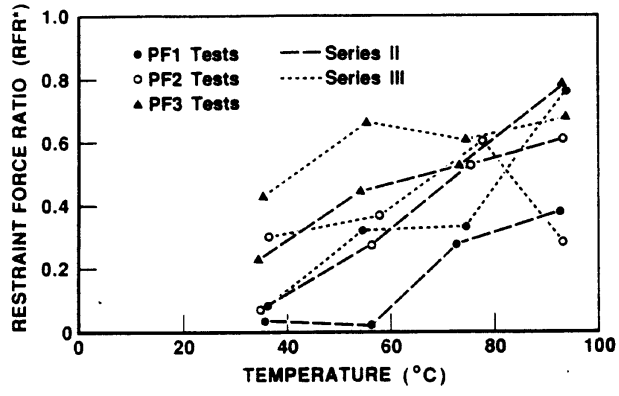

(b) Type II Series II and Series III Tests at 24 Hrs.

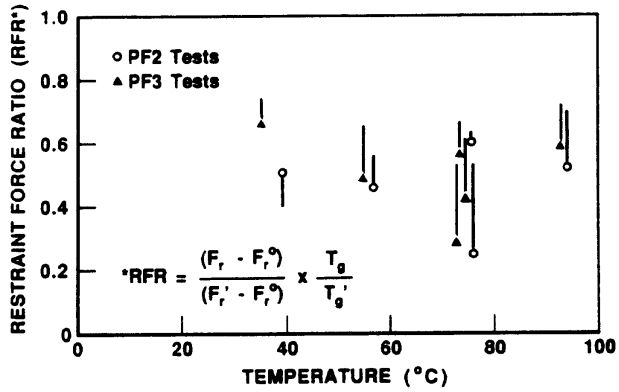

(c) Type II Tests Beyond 24 Hrs.

Fig. 9 — Influence of thermal creep on restraint forces

ratio (RFR) plotted is the percentage change in the thermally induced restraint force, relative to the peak force attained, divided by the percentage change in the thermal gradient over the same period. The temperature plotted is the inside water temperature. Fig. 9(a) shows the relaxation observed in Type II Series tests (tests with low preload in the tie-rods), measured at the end of 24 hr. Fig. 9(b) gives the relaxations observed in Series II and III tests (tests with moderate and high preload in the tie-rods, respectively), also measured at the end of 24 hr. Fig 9(c) shows the results for tests extended beyond 24 hr; the data points represent the ratio at the conclusion of the test, and the lines represent the changes from the 24-hr readings. In the Series I tests, the mean value of the restraint force ratio at the end of 24 hr was 0.701. The extent of relaxation appeared to be fairly uniform across the range of temperatures considered, perhaps being slightly more prominent in the 40 to 60 C range. Thus, in the tests where the forces present were primarily from thermal loading, about a 30 percent decay in forces was observed in the first 24 hr. In the Series II and III tests, the greatest degree of force relaxation was observed at lower temperatures, where the thermal restraint forces were relatively small compared to the coexisting mechanical forces. Here, the relaxation in the first 24 hr was up to 100 percent. As the ratio of thermal to mechanical force increased at higher temperatures, the RFR increased to about the 0.50 level. Thus, in tests with relatively large mechanical-load-induced forces, relaxations in thermal-induced forces in excess of 50 percent occurred over the 24 hr (Note: In tests where only mechanical preloads in the tie-rods were present [i.e., no thermal load], virtually no decay in force was apparent when monitored up to 7 days.) In Fig. 9(c), a significant further relaxation in thermal-restraint force is seen in the time from 24 hr to 7 days. At 24 hr, the mean value of the RFR was 0.611; at the conclusion of the tests (typically 168 hr), it was 0.486. Hence, a further 10 to 15 percent decay occurred. By the end of 7 days, the forces had appeared to stabilize. In addition to relaxation of force, large residual deflections were measured in the models upon removal of load. Both observations point to thermal creep as being a significant factor in influencing short-term response.

Evidence of concrete swelling was clearly observed during the test program. Concrete test cylinders with embedded strain gages placed inside the tank of each model typically began to show signs of progressive straining, (i.e., swelling) when temperatures reached 60 C (140 F). The swelling continued thereafter during both the heating and cool-down periods, resulting in a residual strain of up to $+250\ \mu\epsilon$. Inspecting the cylinders revealed no visible internal or external cracks. This swelling effect was manifested in the test models by residual outward deflections of the columns of approximately 3.5 mm after the first thermal-load cycle of the Type I tests. Additional permanent deformation due to subsequent thermal-load cycles was minimal. Thus, while swelling of concrete under high temperature and moisture conditions appears to be an important factor, additional data are required before more definitive conclusions can be made.

Skin effects were also found to be significant. The outside surfaces of the test models were exposed to ambient air conditions, with several large circulating fans blowing directly onto the surfaces. Yet, significant increases in outside surface temperatures were observed. With an ambient air temperature of 15 C (50 F) and an inside water temperature of 95 C (203 F), for example, the outside surface temperature stabilized at about 35 C (95 F) after 18 hr. Thus, a thermal load of 80 C (144 F) resulted in a final thermal gradient through the structure of 60 C (108 F), although transient thermal gra-

dients as high as 75 C (135 F) were recorded shortly after load application. Hence, the influence of skin effects should not be overlooked in an analysis. (Note: The skin effect on the inside surface, where the contact medium was water, was much less; typically 1 to 2 C.)

THEORETICAL PREDICTIONS OF RESPONSE

An analysis procedure was developed to predict the response of reinforced concrete plane frames subjected to thermal loads (see Reference 7). The computer-based procedure essentially involves a total-load, iterative, secant-stiffness approach to nonlinear frame analysis. It incorporates realistic constitutive relations for the concrete and reinforcement and allows for the consideration of thermal creep, nonlinear thermal gradients, and previous load history. The combined effects of both thermal and mechanical loadings can be analyzed, with the thermal load effects including a consideration of both primary and continuity thermal stresses.

The analytical procedure was found to predict accurately the restraint forces developed in these tests. Consider, for example, the results for Model PF3. Fig. 10 shows the restraint forces measured during Series I, II, and III tests of the Type II test program. The corresponding "theoretical" values obtained using the procedure described are also shown. (Note that predictions were based on thermal conditions corresponding to the peak thermal gradient observed.) In the Series I tests (i.e., low preloads in tie-rods), where the model was in the initial stages of cracking, the theoretical predictions of force are slightly higher than the observed experimental values. This initial overestimation of stiffness may be attributable to internal cracking sustained by the model during Type I testing, which is not accounted for in the theoretical predictions. In the Series II (moderate preload) and Series III (high preload) tests, the theoretical procedure results in slightly low predictions of restraint force. In general, however, both the pattern and the magnitude of the restraint forces are accurately predicted. Predictions of restraint force were also made using ACI-recommended procedures,[5] based on Branson's formula, an empirical relationship for effective stiffness. The predictions obtained for Model PF3 are shown by the "empirical" curves in Fig. 10. Note that these relationships generally underestimate response, but nevertheless provide a reasonable approximation. Predictions based on uncracked section stiffness or fully cracked section stiffness, also shown in Fig. 10, typically result in significant error.

For the 52 Type II tests performed, the ratio of experimental to theoretical restraint force had a mean of 0.905 and a coefficient of variation of 13.6 percent. If the Series I tests performed on Specimen PF1 are omitted (because their results likely were influenced by the preceding Test PF1-C), the mean for the remaining 44 tests then becomes 0.936 with a coefficient of variation of 10.9 percent. The forces were equally well predicted at all levels of thermal gradient. The tendency to slightly overestimate force in the Series I tests is likely

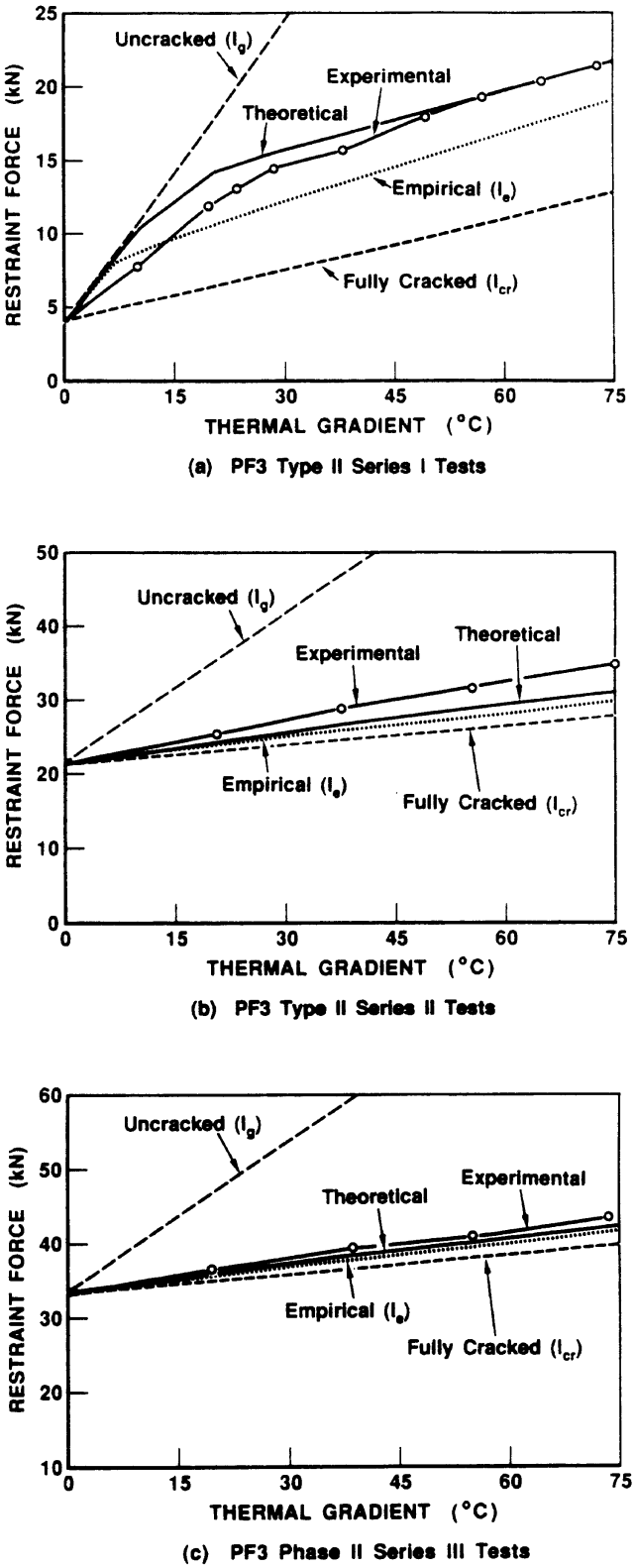

Fig. 10 — Restraint forces in Model PF3 Type II test

related to the tension-stiffening formulation used being somewhat too stiff, as well as to the effects of precracking sustained during Type I tests.

The correlation between predicted and observed deformations in the beam were examined. For the Type II tests, the ratio of experimental to theoretical deflection at the beam midspan showed considerable scatter with a mean of 0.887 and a coefficient of variation of 53.9

percent. However, it must be noted that the beam deflections in the restrained models were very small (typically less than 0.5 mm), extremely sensitive to the progession of cracking throughout the structure, and strongly influenced by time-related effects (i.e., thermal creep). In Type I tests, deflections were much more accurately predicted (mean 1.032, coefficient of variation 2.9 percent). The beam elongations, although influenced by cracking, did not depend to any great extent on the overall structural interactions. Hence, the ratio of experimental to predicted deformation in this sense was much less scattered, with a mean value of 1.049 and a coefficient of variation of 16.6 percent.

The ability of the theoretical model to predict strains in the reinforcing bars was also examined. The strains in the top (compression) bars were reasonably well predicted, with the ratio of experimental to theoretical values having a mean of 0.974 and a coefficient of variation of 26.8 percent. In the bottom (tensile) reinforcement, the scatter was more prevalent with corresponding values of 0.858 and 50.4 percent. Large amounts of scatter in the strain readings are expected because of the stochastic nature of cracks forming in the concrete. Strains in reinforcing bars are significantly higher at crack locations than they are in regions between cracks. Strain gages measure localized strains, and thus are sensitive to crack location. The strains computed in the theoretical analyses, on the other hand, represent average values. Further, the experimentally derived strains are subject to error in the factoring out of the relatively large thermal-strain component.

A simple model for thermal creep, based on a rate process theory and using a formulation proposed by Marechal,[9] was implemented into the analytical procedure. Analyses were conducted to determine if the relaxation in restraint forces observed in the Type II tests could be adequately accounted for on this basis. The creep formulation used accounted for only a small portion of the relaxation observed. An improved formulation that takes into account the influence of stresses acting in the concrete appears necessary.

CONCLUSIONS

The test program successfully provided an extensive database for calibrating theoretical procedures for the analysis of reinforced concrete stuctures under thermal loads. Observations or conclusions arising from the program include the following:

1. Thermal loads imposed on a reinforced concrete structure can induce significant levels of deformation, stressing, and cracking. Where present, thermal loads should be expressly considered in the analysis and design of a stucture.

2. The internal forces induced in a structure by thermal loads are heavily dependent on structural stiffness. Accordingly, factors such as relative member dimensions, reinforcement details, coexisting mechanical load, concrete tensile strength, and concrete tension stiffening effects have a great influence and should be considered.

3. The force and deformation developed at a particular location in a structure are affected by the overall structural response to the thermal loads. Thermally induced deformations tend to concentrate at weaker regions in the structure and can result in excessive cracking, yielding, and development of leakage paths.

4. The primary thermal stresses induced in an unrestrained structure can be sufficient to cause internal cracking. This effect can subsequently influence structure stiffness or the development of leakage paths.

5. The forces, strains, and deformations arising from thermal loads tend to be greatest shortly after the peak thermal loads are achieved, regardless of the nonlinearity of the thermal gradient through the structure. Hence, the difference in temperature between opposite surfaces is the dominant factor.

6. Thermal creep results in a significant relaxation of internal restraint forces in as short a time as 24 hr. Large permanent deformations can also result.

7. The ductility and ultimate load capacity of a reinforced concrete section is not significantly affected at temperatures lower than 100 C. The material properties of the concrete and reinforcement can be assumed to be unchanged. However, swelling of the concrete can be triggered by moderately high temperatures and high moisture conditions.

8. The short-term response of structures to thermal loads can be predicted accurately using nonlinear frame-analysis procedures. Aspects of response such as restraint forces, cracking, deflections, and reinforcement stresses can be computed reasonably well.

9. Analyses based on an effective stiffness formulation using ACI-recommended procedures provide reasonable predictions in lieu of more rigorous nonlinear analyses.

10. Analysis procedures based on uncracked or fully cracked conditions are inadequate. Also, procedures based on a section analysis only cannot account for load redistributions or deformation concentrations which can be significant.

ACKNOWLEDGMENTS

The experimental work described in this paper was funded by, and conducted at the facilities of Ontario Hydro. The analytical program formulation, and analysis of test data, was funded by Ontario Hydro and by the Natural Sciences and Engineering Research Council of Canada.

NOTATION

A_s = cross-sectional area of bottom longitudinal reinforcement
A_s' = cross-sectional area of top longitudinal reinforcement
A_v = cross-sectional area of shear reinforcement
b = width of member cross section

d = position of bottom longitudinal reinforcement
d' = position of top longitudinal reinforcement
F_t = restraint force in tie-rods at time t
F_t^i = initial restraint force in tie-rods
F_t' = peak restraint force in tie-rods
h = depth of member cross section
s = spacing of shear reinforcement
t = time elapsed from time of thermal loading
T_1 = initial inside surface temperature
T_1' = inside surface temperature at time t
T_2 = initial outside surface temperature
T_2' = outside surface temperature at time t
T_g = thermal gradient ($T_g = T_1' = T_2'$)
T_g' = peak thermal gradient
T_i = inside (water) temperature
T_o = outside (air) temperature
δ_a = axial elongation of beam member
δ_b = deflection of beam at midspan (downward positive)
δ_c = relative deflection of columns at tie-rods (outward positive)
ϵ_{sbb} = strain in beam bottom reinforcing bar at midspan
ϵ_{sbt} = strain in beam top reinforcing bar at midspan
ϵ_{scb} = strain in column outside reinforcing bar at base
ϵ_{sci} = strain in column inside reinforcing bar at base

REFERENCES

1. Priestley, M.J.N.,"Thermal Stresses in Concrete Structures," *Proceedings,* Stuctural Concrete Conference, Toronto, 1981, pp. 255-283.

2. Elbadry, Mamdouh, and Ghali, Amin, "Thermal Stresses and Cracking of Concrete Bridges," ACI JOURNAL, *Proceedings* V. 83, No. 6, Nov.-Dec. 1986, pp. 1001-1009.

3. Elgaaly, M., "Thermal Gradients in Beams, Walls, and Slabs," ACI JOURNAL, *Poceedings* V. 85, No. 1, Jan.-Feb. 1988, pp. 76-81.

4. ACI Committee 349, "Reinforced Concrete Design for Thermal Effects on Nuclear Power Plant Structures," (ACI 349.1R-80), American Concrete Institute, Detroit, 1980, 30 pp.

5. ACI Committee 435, "State-of-the-Art Report on Temperature-Induced Deflections of Reinforced Concrete Members," (ACI 435.7R-85), American Concrete Institute, Detroit, 1985, 14 pp.

6. Bhat, P.D., and Vecchio, F. J., "Design of Reinforced Concrete Containment Structures for Thermal Gradients Effects," *Proceedings*, 7th Conference on Structural Mechanics in Reactor Technology, Chicago, Aug. 1983, Paper J4/1, pp. 171-178.

7. Vecchio, Frank J., "Nonlinear Analysis of Reinforced Concrete Frames Subjected to Thermal and Mechanical Loads," *ACI Structural Journal,* V. 84, No. 6, Nov.-Dec., pp. 492-501.

8. Vecchio, F. J., "Thermal Gradients Test Program: Summary Report," *Research Division Report* No. 88-230-H, Ontario Hydro, Toronto, Nov. 1988, 73 pp.

9. Marechal, J. C., "Creep of Concrete as a Function of Temperature," *Concrete for Nuclear Reactors,* SP-34, American Concrete Institute, Detroit, 1972, pp. 547-564.